SAND2009-0049C

European Wind Energy Conference & Exhibition 2009
Parc Chanot, Marseille, France 16-19 March 2009

Abstract No. 223

ACTIVE AERODYNAMIC BLADE CONTROL DESIGN FOR LOAD REDUCTION ON LARGE WIND TURBINES TO INCREASE ENERGY CAPTURE

David G. Wilson*, Dale E. Berg, Mathew F. Barone, Jonathan C. Berg, Brian R. Resor and Don W. Lobitz
Energy Systems Analysis*/ Wind Energy Technology
Sandia National Laboratories, P.O. Box 5800
Albuquerque, New Mexico 87185–1108
Email: {dwilso,deberg,mbarone,jcberg,brresor,dwlobit}@sandia.gov

ABSTRACT

Through numerical simulations that use trailing edge flaps as active aerodynamic load control devices on wind turbines that range from 0.6MW-5MW rated power, a 20-32% reduction in fatigue loads or bending moments was achieved. This allows the turbine blade lengths to be increased, without exceeding original fatigue damage on the system, resulting in larger swept rotor area. This study developed and tested several independent flap control designs (including tip deflection and tip rate deflection feedback) that seamlessly integrated in with existing pitch control strategies that reduced loads sufficiently to allow 10% rotor extension and increased energy capture of approximately 10% (see reference [1] for methodology).

1 Introduction

Wind turbines are large complex dynamically flexible structures that must operate under very turbulent and unpredictable environmental conditions where efficiency and reliability are highly dependent upon a well designed control strategy. The possibility to quickly influence aerodynamic loads acting on the individual blades allows for a hybrid pitch control objective that includes a high frequency dynamic attenuation component with respect to fatigue load reduction. Active aerodynamic devices are potential candidates for this component.

With wind turbine blades getting larger and heavier, can the rotor weight be reduced by adding active devices? Can active control be used to reduce fatigue loads? Can energy capture in low wind conditions be improved? These are some of the questions that are being addressed in our research program. Specifically our research goal is to understand the implications and benefits of active blade control in Region III. To modify the blade/turbine active load control one can change blade aerodynamic characteristics through: i) surface blowing/suction, ii) VG's, surface heating, plasma, etc., or iii) changes in section shape (aileron, smart materials, microtabs).

In practical applications the reduction of structural fatigue loads is important for the continued operation of wind turbines over a lifetime. One example of these types of loads is reported by Kelley, et.al. [2], where the impact of coherent inflow turbulence on the wind turbine dynamic response is identified.

> *Previous field experimentation showed greatest structural fatigue damage tends to occur during nighttime hours from coherent turbulence that develops in the stable, nocturnal atmospheric boundary layer. Under such conditions, intense vertical wind shear and temperature gradients create resonant flow fields capable of imparting short-period loading and vibrational energy as wind turbine rotor blades pass through regions of organized or coherent turbulence. This energy is subsequently propagated throughout the remainder of structure, where it is often locally dissipated [2].*

A time-frequency spectral decomposition of the root flapwise load encountering coherent turbulent structure indicated that the highest level of dynamic stress energy occurred in the frequency range consisting of the first and second flap bending modes [2, 3]. It was determined that the number of stress reversals increase as the rotor passes through coherent turbulent struc-

*Address all correspondence to this author.

tures [2]. Due to the nature of the load application and the existence of small values of structural damping, a potentially significant transient storage of vibrational energy must be dissipated. The potential of a modal dynamic amplification that may exist could contribute to a lower than designed component service lifetime [2]. Active aero devices are a good candidate to help reduce these detrimental effects of high frequency dynamics and fatigue loads on wind turbines.

For wind turbines to continue a reduction in cost of energy technical advances from several areas will be required. In the area of aerodynamics, controls, and sensors several researchers have started to investigate the benefits of using advanced control for wind turbine rotor aerodynamics and geometry. In McCoy and Griffin [4] two major categories of rotor aerodynamic modifications were investigated. This included active aerodynamic devices and actively controlled retractable blade rotors. Both studies showed indications of cost savings through reduced system loads and increased energy capture. van Dam et. al. [5–7], has investigated both computationally with CFD investigations and through experimental wind tunnel testings the preliminary feasibility of microtabs for active load control. Andersen, et.al. [8] have developed deformable trailing edge geometry and control algorithms which also showed fatigue load reduction for both the flapwise blade root moments and the tower root moments. By enabling the trailing edge to move quickly and independently at the outboard portion of the blade then local fluctuations in the aerodynamic forces can be compensated with these trailing edge flaps. Additionally, Barlas and van Kuik [9] give an overview of smart rotor control technology for wind turbines.

In this study the authors investigate the combined control performance of several types of trailing-edge devices that include micro-tabs, morphing trailing edges (5%, 10%, 20% of blade chord), and conventional trailing edge flaps in conjunction with collective pitch control to provide effective load alleviation for a range of variable-speed, variable-pitch wind turbines (600 kW NREL CART, 1.5MW WindPACT, and 5.0 MW NREL Offshore). This study demonstrates that advanced independent flap control based on either tip deflection or tip deflection rate measurements combined with existing blade pitch control strategies is advantageous for loads reduction. In addition, the control designer must be aware of and keep to a minimum the flap bending and torsion coupling which may become more apparent as the turbines increase in rotor diameter.

This paper is divided into six sections. Section 2 provides an overview of the active aerodynamic devices and performance employed on the wind turbines. Section 3 defines the three wind turbine models. Section 4 develops the hybrid control system for both the pitch and active aerodynamic controllers. Section 5 presents the numerical simulation results for the three wind turbines studied and Section 6 summarizes the results with concluding remarks.

2 Active Aerodynamic Devices and Performance

2.1 Characteristics

The aerodynamic properties of blade sections with active aerodynamic devices required by the FAST code were obtained using the ARC2D code [10] Computational Fluid Dynamics (CFD) code. The ARC2D code, a two-dimensional Navier-Stokes solver, was used to generate aerodynamic lookup tables for lift coefficient, drag coefficient, and pitching moment coefficient for each airfoil geometry of interest, including configurations where the microtab or morphed shape was activated. The CFD results were obtained using the Spalart-Allmaras turbulence model, with specified upper and lower surface boundary layer transition locations. The transition locations were estimated using the XFOIL viscous panel code [11]. The use of CFD allowed for a consistent method for determining changes in airfoil performance with the non-trivial shape changes associated with the active aero devices. The time required to generate meshes for the CFD calculations of many different shapes was greatly reduced by the use of an automated mesh-generation tool [12]. CFD solutions were obtained over an angle of attack range of -14 degrees to +20 degrees; the airfoil tables were then pre-processed using the AirfoilPrep spreadsheet [13], which applies the Viterna method to expand the performance tables to the full 360 degree range of angles of attack required by the FAST/Aerodyn codes.

2.2 Microtab concepts and background

The microtab concept comes from an evolutionary development of the Gurney flap (see Liebeck [14]). The tab is deployed near the trailing edge of the airfoil to a height on the order of the boundary layer thickness (approximately 1% of chord), as shown in Fig. 1. Some of the desirable features include: i) significant increases in C_L, ii) relatively small increase in C_D, and iii) proper sizing can increase L/D. Further details of the microtab concept can be found in reference [15].

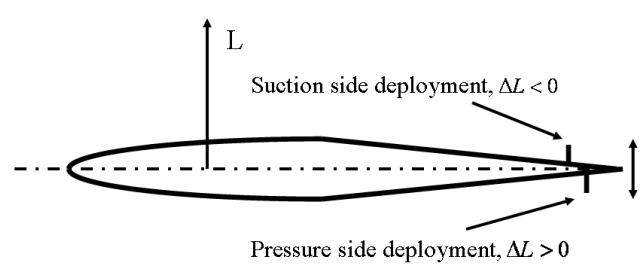

Figure 1. Microtab concept based on Kutta Condition (van Dam [15])

The specific microtab characteristics, based on experimental results, are given in Fig. 2 for both the lift and drag profiles, respectively. In the next section these profiles are used as AeroDyn [16] inputs to the FAST/Simulink [17] dynamics and controls simulator.

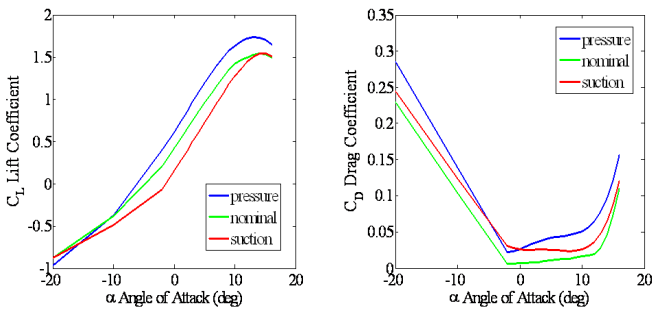

Figure 2. Microtab C_L and C_D Profiles used as input to AeroDyn software

2.3 Morphing wing concept

FlexSys Inc., of Ann Arbor, Michigan has developed and flight tested a technology that enables them to morph a wing trailing edge [18, 19]. That is, they can smoothly and quickly distort the trailing edge of a wing to form an effective flap, while avoiding the discontinuities in the upper and lower wing surfaces, the hinge line and the attendant air gap that are associated with traditional flaps. The morphed flap has a lift characteristic comparable to that of a conventional flap, but with a much reduced drag increment due to flap deflection. The morphing wing cross-section profiles are shown in Fig. 3.

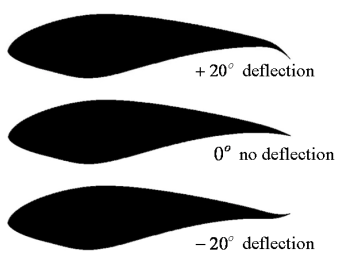

Figure 3. Morphing wing trailing edge concept ([18])

2.4 Conventional trailing edge flaps

An airfoil with a conventional flap consists of two distinct sections - the fixed leading edge section of the airfoil and a rigid trailing edge section that rotates about the spanwise hinge attached to the leading edge section (see Fig. 4). This type of flap has a distinct hinge line, an associated clearance gap (through which air can leak, causing loss of lift and generating noise) and sharp changes or discontinuities in both the upper and lower surfaces of the airfoil. As a result of these characteristics, the airflow over the airfoil with a deflected flap tends to separate at low angles of attack and create excessive drag.

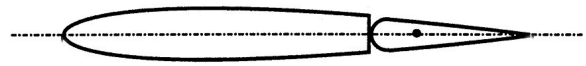

Figure 4. Conventional trailing edge airfoil

3 Turbine models

The wind turbine models utilized in this work are in the public domain and include the NREL 600 kW 3-bladed Controls Advanced Research Turbine, the 1.5 MW WindPACT turbine, and the NREL/UpWind 5 MW Offshore wind turbine (see Table 1). All turbines are upwind, with variable speed, and collective pitch control. Each turbine has been modified to include an Active Aerodynamic Load Control (AALC) system to work with the existing collective pitch control system.

Our performance index goal is to maintain maximum power output while minimizing blade root bending moment oscillations about a mean during turbulent wind conditions. The NREL TurbSim code generates NTM IEC Type A turbulence wind fields up to 10 minutes in duration for mean wind speeds ranging from 5 m/s to 24 m/s. The NREL FAST/AeroDyn/Simulink wind turbine dynamics/controls simulation code was employed for the control system studies.

Table 1. Wind turbine model characteristics

Turbine	NREL CART	WindPACT	NREL Offshore
Rating	600kW	1.5 MW	5.0MW
Rotor size	42.7m	65.9m	126m
Blade len.	20.0m	31.3m	61.5m
V_{rated}	13 mps	12.5 mps	11.4 mps
$V_{cut-out}$	20 mps	22.5 mps	25 mps
# Blades	2	3	3
AALC	microtabs	morphing wing	conventional flaps

4 Hybrid Pitch/Active Aero Control System Design

In Region III, most wind turbines have a collective and/or an individual pitch control scheme to keep the turbine operating at peak output power while at higher wind speed conditions. One of the initial goals of this project was to minimize the redesign of the control system yet understand the benefits of introducing active aerodynamic devices on the blades. Therefore, a hybrid controller that combines a traditional pitch control system with the microtab, morphing wing, or conventional flap control system was developed. The pitch control system consists of an

existing Proportional-Integral (PI) feedback design [20] and is part of all the wind turbines that were investigated. The active aerodynamic devices all use the same control system consisting of a Proportional-Derivative (PD) feedback design as discussed in [21]. The PD controller uses tip deflection as the feedback signal. In addition, a nominal operating point is included as a reference input signal or

$$\beta_{actuator} = -K_P(y_{tip} - y_{tip_{nom}}) - K_D \frac{\partial y_{tip}}{\partial t}. \quad (1)$$

In addition, a second control law was also tested on the 1.5MW WindPACT machine and is based on rate feedback only. In this case the tip deflection rate would be required and in the above equation, $K_P = 0$. In this case, the controller acts as a regulator with respect to tip deflection rate. Each control law was shown to be affective in alleviating loads.

The FAST/Simulink modeling environment [17] was used to evaluate the hybrid control system performance at 18 mps wind condition in Region III (see Fig. 5 for actual IEC turbulent wind conditions used in simulation). Several conventional 10 min turbulent wind conditions were investigated. For these discussions a time splice of 100 seconds are displayed in all time domain responses. The baseline CART FAST model was modified to incorporate the microtab control system and is shown in Fig. 6. The block in green is the CART plant while all the control system feedback loops are implemented in the Simulink block diagram (see Fig. 6). The same process was used for the 1.5MW WindPACT wind turbine utilizing the morphing wing trailing edge devices with 20% blade chord modifications. For the 5MW offshore wind turbine, conventional flaps were employed.

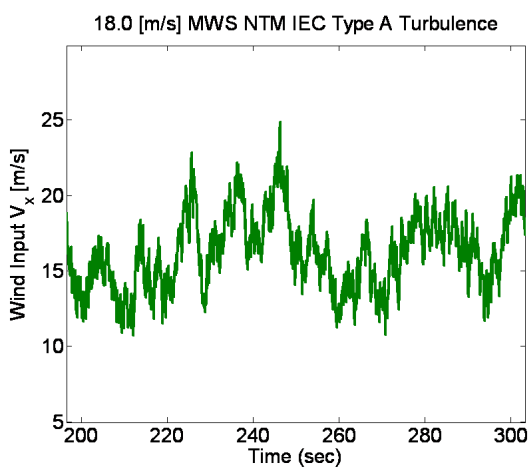

Figure 5. Wind input file used for all WT discussions.

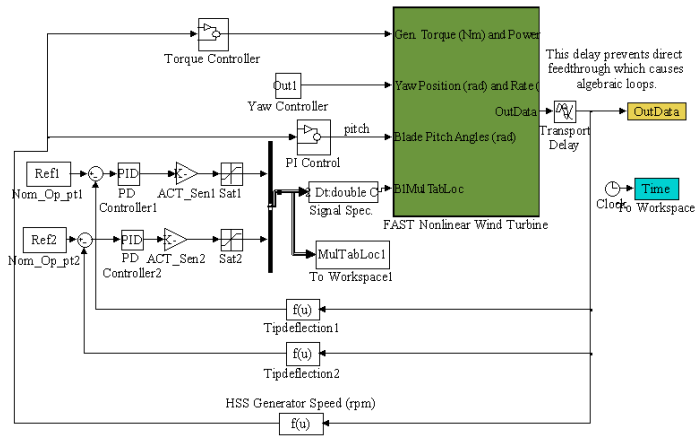

Figure 6. Dynamic simulation environment: FAST with augmented pitch and microtab control systems for the CART machine

5 Numerical Simulation Results

5.1 600kW CART machine

The numerical simulation results from the FAST runs are reported for both *MicroTabs* (shown in blue) and *No MicroTabs* (shown in red) cases. Figure 8 shows the blade 1 root flap moment response (left) and the blade one tip deflection response (right). For the flap moment a reduction of the peak moments of 20% along with a reduction in overall tip deflection can be observed (see Table 2).

Figure 9 shows the blade 1 pitch angle responses (left) along with the microtab sequencing output (right). Figure 10 shows the generator power response (left) and the rotor speed response (right). Both of these responses maintain power and speed while using microtabs.

Since the combined control systems can potentially couple other degrees-of-freedom associated with the overall system, the tower modes were also checked. Figure 11 shows the tower base side-to-side moment response (left) and the tower base fore-aft moment response (right). Both with and without the microtabs the responses are along the same order of magnitude. In addition, the LSS torque (see Fig. 12 left) and tower top/yaw bearing yaw moment (right) responses are checked to ensure that loads remain level while activating the AALC devices.

5.2 1.5MW WindPACT wind turbine

The numerical simulation results from the FAST runs are reported for both morphing wing with 20% blade chord *Flaps 20% C* (shown in blue) and no morphing *No Flaps* (shown in red) cases. Figure 13 shows the blade 1 root flap moment response (left) and the blade one tip deflection response (right). For the flap moment a reduction of the peak moments of 32% along with a reduction in overall tip deflection can be observed (see Table 2). Figure 14 shows the blade 1 pitch angle responses (left)

along with the morphing wing actuator rotation (right). Figure 15 shows the generator power response (left) and the rotor speed response (right). Both of these responses maintain power and speed while using the morphing wing trailing edge.

Figure 16 shows the tower base side-to-side moment response (left) and the tower base fore-aft moment response (right). Both with and without the morphing wing device the responses are along the same order of magnitude. In addition, the LSS torque (see Fig. 17 left) and tower top/yaw bearing yaw moment (right) responses are maintaining level loading while activating the AALC devices.

The same series of runs were conducted using the rate feedack control system. The numerical results compiled from the FAST runs are shown in Fig. 18 through Fig. 22. Similar conclusions can be stated as stated in the previous set of results. The peak moments associated with flap moment response (see Fig. 18 - left) gave a reduction of 25.4%, see Table 2, for overall comparisons.

Further data reduction shown in Figure 7 for the composite rainflow cycle counting results for data gathered at 7, 9, 11, 18 and 24 m/s average windspeeds (six seeds at each windspeed) demonstrates actual reduction in fatigue loads. The windspeed data were combined using a Rayleigh wind speed distribution with average of 5.5 m/s. The composite data show that the numbers of cycles accumulated above 2000 kN-m were eliminated with the use of AALC. Also the numbers of cycles at lower moments were reduced from the baseline case at all cycle amplitudes.

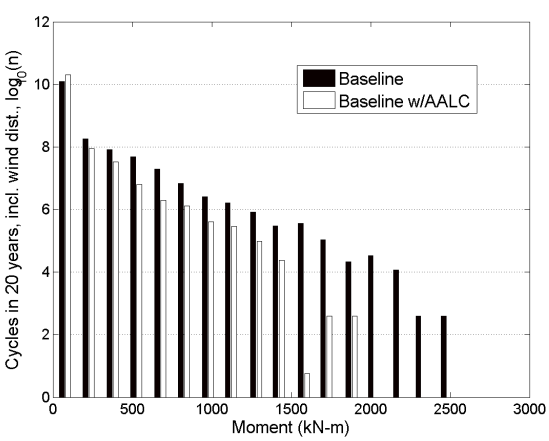

Figure 7. Blade root flap moment rainflow cycle counting results for baseline and active aerodynamic load control (AALC) configurations. 20% chord length, $\pm 10^\circ$ max. actuation, PD blade tip displacement control.

5.3 5 MW offshore wind turbine

The numerical simulation results from the FAST runs are reported for both conventional *Flaps* (shown in blue) and *No Flaps* (shown in red) cases. The numerical results compiled from the FAST runs are shown in Fig. 23 through Fig. 27. Similar conclusions can be stated as stated in all the previous sets of results. The peak moments associated with flap moment response (see Fig. 23 - left) gave a reduction of 19.97%, see Table 2, for overall comparisons.

Table 2. Root Bending Moment Tabulated Results

WT (MW) (size)	Mean (kNm)	STD (kNM) (no flaps / flaps)	% Red. STD
0.6	206	53.32 / 42.25	20.77
1.5	603	294 / 199.5	32.16
1.5 RC	603	294 / 219	25.40
5.0	4714	2350 / 1880	19.97

6 Conclusions

This paper has shown the feasibility for employing active aerodynamic devices for load alleviation. Microtabs were tested with the 600kW NREL CART machine. A morphing wing trailing edge device with 20% chord was tested with the 1.5 MW WindPACT wind turbine and conventional flaps were tested with the 5 MW NREL Offshore wind turbine. For the 1.5MW WindPACT wind turbine, both a PD feedback controller, based on tip deflection, and a rate feedback controller base on tip rate deflection were shown to be effective strategies for load reduction. The general trend for all turbines, showed a reduction in root flap bending moments, from 20-32% reduction in the standard deviation oscillations from the mean value. This translates to reduction in the fatigue loading on the wind turbines. It has been demonstrated that active aerodynamic devices may provide substantial benefit for future wind turbine designs. For example, the designer can include: i) increased effective rotor size, ii) extend potential life expectancy and reliability, and iii) ultimately reduce the cost-of-energy of future large wind turbine machines. By reducing the fatigue loads with the active aerodynamic devices while keeping drivetrain and tower loads level, the rotor can be grown by increasing the blades (by approximately 10%) until the original fatigue load levels are reached. This resulted in approximately 10% increase in energy capture [1]. A methodology for reducing loads and fatigue such that the designer can then *grow the rotor*, by significantly increasing the blade lengths on the turbine, and effectively increase energy capture is further developed in [1].

ACKNOWLEDGMENT

Sandia National Laboratories is a multiprogram laboratory operated by Sandia Corporation, a Lockheed Martin Company, for the U.S. Department of Energy's National Nuclear Security Administration under contract DE-AC04-94AL85000.

REFERENCES

[1] Berg, D.E., Wilson, D.G., Berg, J., Resor, B., Barone, M., Kota, S., Ervin, G., and Maric, D., *The Impact of Active Aerodynamic Load Control on Wind Energy Capture at Low Wind Speed Sites*, accepted for publication, European Wind Energy Conference & Exhibition, France, March, 2009.

[2] Kelley, N.D., et. al., *The Impact of Coherent Turbulence on Wind Turbine Aeroelastic Response and Its Simulation*, WindPower 2005 Conference, NREL/CP-500-38074, August 2005

[3] Jonkman, J. and Cotrell, J., *Demonstration of the Ability of RCAS to Model Wind Turbines*, National Renewable Energy Laboratory. Golden, CO. NREL/TP-500-34632, 2003.

[4] McCoy, T.J. and Griffin, D.A., *Active Control of Rotor Geometry and Aerodynamics: Retractable Blades and Advanced Devices*, AWEA WINDPOWER 2007 Conference, Los Angeles, CA., June 4-6, 2007.

[5] Yen, D., van Dam, C.P., Smith, R.L. and Collins, S.D., *Active Load Control for Wind Turbine Blades Using MEM Translational Tabs*, Proceedings of the 2001 ASME Wind Energy Symposium (AIAA 2001-0031), Reno, Nevada, January 2001.

[6] Yen Nakafuji, D.T., van Dam, C.P., Michel, J., Morrison, P. *Load Control for Turbine Blades: A Non-Traditional Microtab Approach,* Proceedings of the 2002 ASME Wind Energy Symposium (AIAA 2002-0054), Reno, Nevada, January 2002.

[7] van Dam, C.P., et. al., *Computational and Experimental Investigation into the Effectiveness of a Microtab Aerodynamic Load Control System*, Sandia National Laboratories, August, 2004, Draft.

[8] Andersen, P.B., et. al., *Integrating Deformable Trailing Edge Geometry in Modern Mega-Watt Wind Turbine Controllers*, EWEA 2008 European Wind energy Conference & Exhibition, Belgium March 31 - April 3, 2008.

[9] Barlas, T.K. and van Kuik, G.A.M., *State of the Art and Prospectives of Smart Rotor Control for Wind Turbines*, The Science of Making Torque from Wind, J. of Physics: Conference Series 75, 2007.

[10] Pulliam, T. H., *Efficient Solution Methods for the Navier-Stokes Equations*, Lecture Notes for the von Karman Institute for Fluid Dynamics Lecture Series: Numerical Techniques for Viscous Flow Computation in Turbomachinery Bladings, von Karman Institute, Rhode-St-Genese, Belgium., 1986.

[11] Drela, M. and Giles, M.B. *Viscous-Inviscid Analysis of Transonic and Low Reynolds Number Airfoils*, AIAA J, 25(10):1347-1355, 1987.

[12] Yoo, S.Y. *Integrated Method of CFD and Grid Generation for Automatic Generation of Airfoil Performance Tables*, M.S. Thesis, Mechanical and Aeronautical Engineering Department, University of California-Davis, 2008.

[13] NWTC Design Codes (AirfoilPrep by Dr. Craig Hansen). http://wind.nrel.gov/designcodes/preprocessors/airfoilprep/. Last modified 16-January-2007; accessed 16-January-2007.

[14] Liebeck, R.H., *Design of Subsonic Airfoils for High Lift*, J. of Aircraft, Vol. 15, No. 9, September 1978, pp. 547–561.

[15] van Dam, C.P., et. al., *Active Load Control of Wind Turbine Blades Using Small Tabs or Flaps*, AWEA WINDPOWER 2007, Los Angeles, CA., June 4-6, 2007.

[16] Laino, D.J. and Hansen, A.C., *AeroDyn User's Guide*, prepared for NREL, Windward Engineering, 2002.

[17] Jonkman, J.M. and Buhl, Jr., M.L., *FAST User's Guide*, NREL Technical Report, NREL/EL-500-38230, August 2005.

[18] Kota, S., Hetrick, J.A., Osborn, R., Paul, D., Pendleton, E., Flick, P., and Tilmann, C., *Design and Application of Compliant Mechanisms for Morphing Aircraft Structures*, Smart Structures and Materials 2003: Industrial and Commercial Applications of Smart Structures Technologies, Eric H. Anderson, Editor, Proceedings of SPIE Vol. 5054, 2003.

[19] J.A. Hetrick, J.A., Osborn, R.F., Kota,S., Flick, P.M., Paul, D.B., *Flight Testing of Mission Adaptive Compliant Wing*, 48th AIAA/ASME/ASCE/AHS/ASC Structures, Structural, April 2007, Honolulu, Hawaii, AIAA 2007-1709.

[20] Wright, A.D., *Modern Control Design for Flexible Wind Turbines*, NREL Technical Report, NREL/TP-500-35816, July 2004.

[21] Basualdo, S., *Load Alleviation on Wind Turbines using Variable Airfoil Geometry (A 2-D Analysis)*, Technical University of Denmark, Fluid Mechanics Section, Feb. 2004.

APPENDIX: Wind Turbine FAST Simulation Results

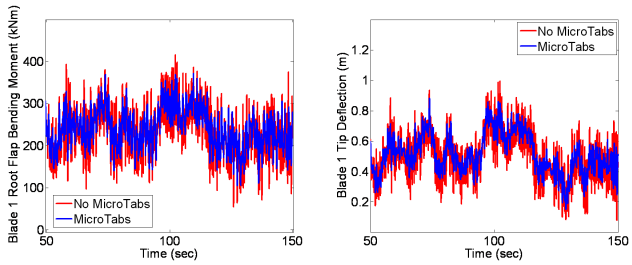

Figure 8. Numerical simulation results 600kW WT: blade 1 root flap moment response (left) and blade 1 tip deflection response (right)

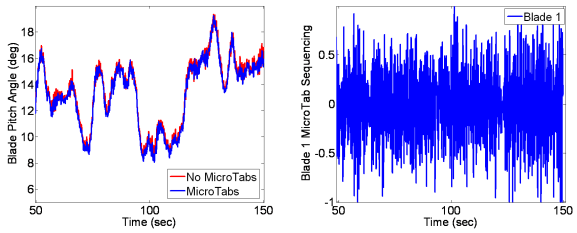

Figure 9. Numerical simulation results 600kW WT: blade 1 pitch angle response (left) and blade 1 microtab sequencing (right)

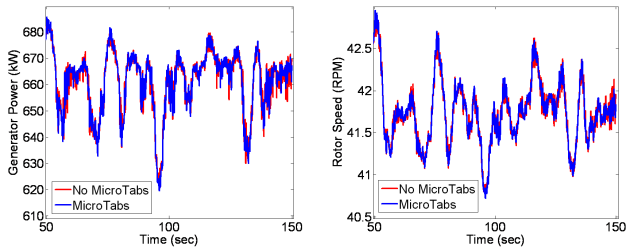

Figure 10. Numerical simulation results 600kW WT: generator power response (left) and rotor speed response (right)

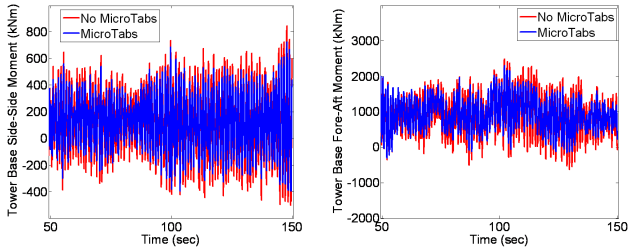

Figure 11. Numerical simulation results 600kW WT: tower base side-to-side moment response (left) and tower base fore-aft moment response (right)

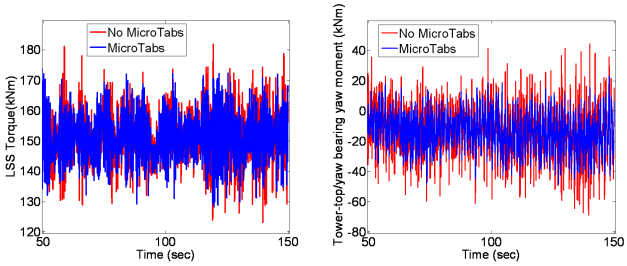

Figure 12. Numerical simulation results 600kW WT: LSS torque response (left) and tower top/yaw bearing yaw moment response (right)

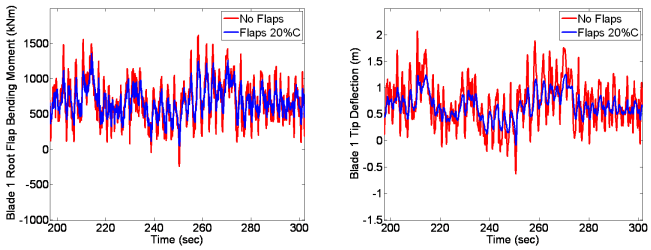

Figure 13. Numerical simulation results 1.5MW WT: blade 1 root flap moment response (left) and blade 1 tip deflection response (right)

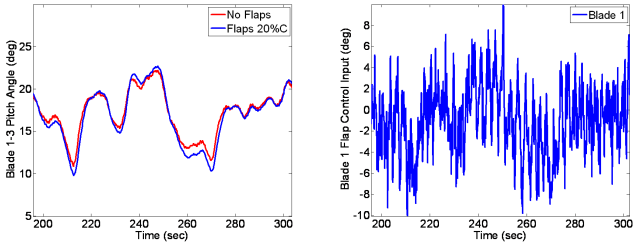

Figure 14. Numerical simulation results 1.5MW WT: blade 1 pitch angle response (left) and blade 1 morphing wing rotation (right)

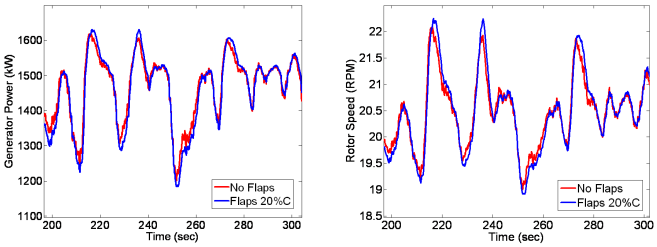

Figure 15. Numerical simulation results 1.5MW WT: generator power response (left) and rotor speed response (right)

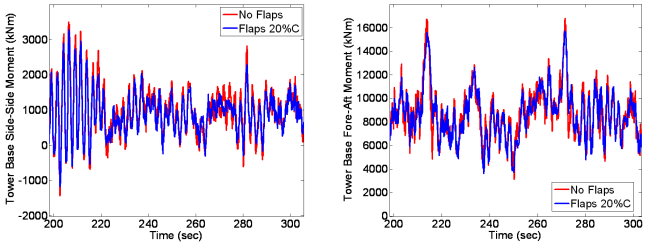

Figure 16. Numerical simulation results 1.5MW WT: tower base side-to-side moment response (left) and tower base fore-aft moment response (right)

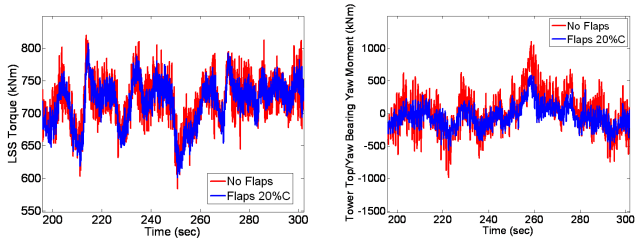

Figure 17. Numerical simulation results 1.5MW WT: LSS torque response (left) and tower top/yaw bearing yaw moment response (right)

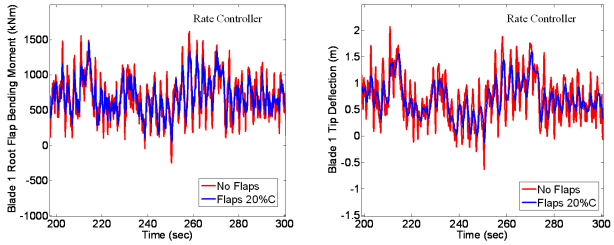

Figure 18. Numerical simulation results 1.5MW WT: blade 1 root flap moment response (left) and blade 1 tip deflection response (right)

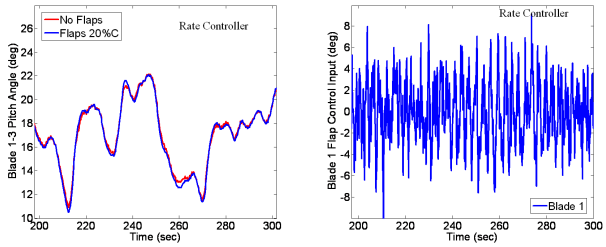

Figure 19. Numerical simulation results 1.5MW WT: blade 1 pitch angle response (left) and blade 1 morphing wing rotation (right)

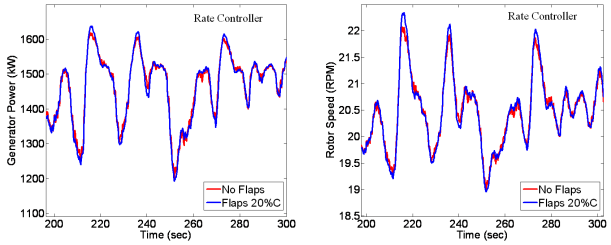

Figure 20. Numerical simulation results 1.5MW WT: generator power response (left) and rotor speed response (right)

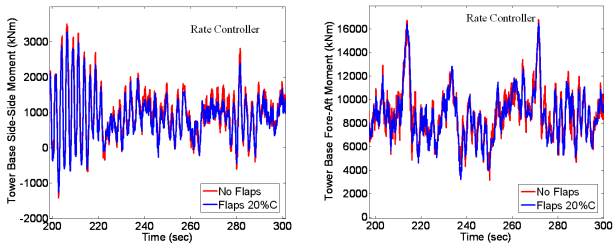

Figure 21. Numerical simulation results 1.5MW WT: tower base side-to-side moment response (left) and tower base fore-aft moment response (right)

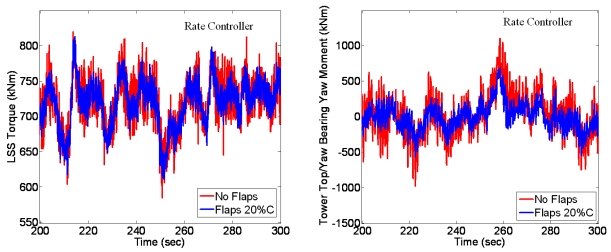

Figure 22. Numerical simulation results 1.5MW WT: LSS torque response (left) and tower top/yaw bearing yaw moment response (right)

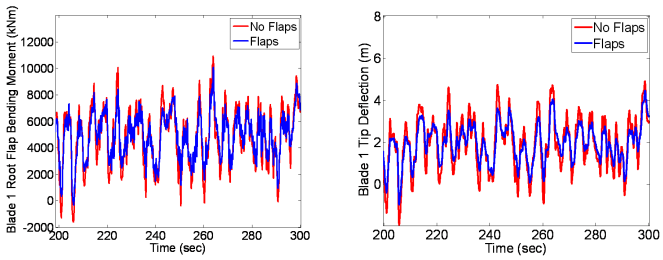

Figure 23. Numerical simulation results 5MW WT: blade 1 root flap moment response (left) and blade 1 tip deflection response (right)

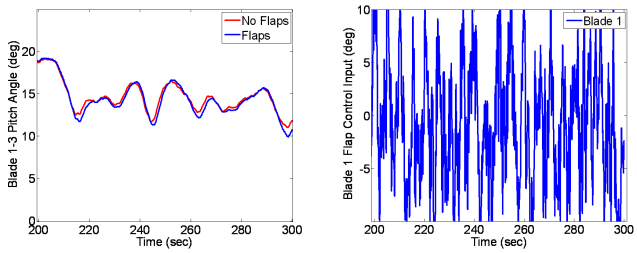

Figure 24. Numerical simulation results 5MW WT: blade 1 pitch angle response (left) and blade 1 conventional flap rotation (right)

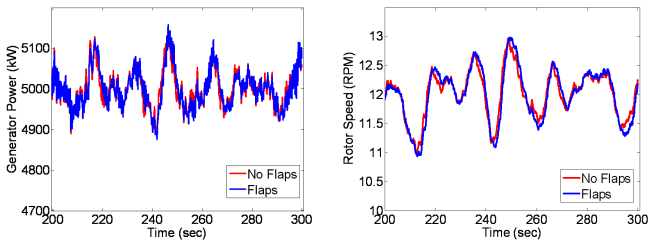

Figure 25. Numerical simulation results 5MW WT: generator power response (left) and rotor speed response (right)

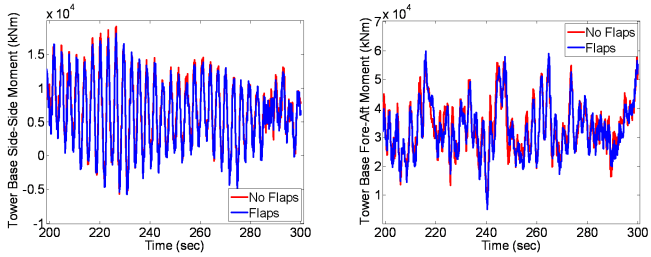

Figure 26. Numerical simulation results 5MW WT: tower base side-to-side moment response (left) and tower base fore-aft moment response (right)

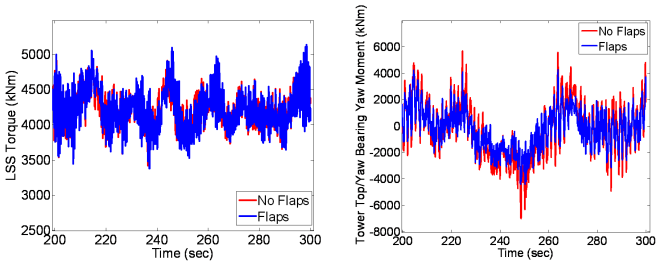

Figure 27. Numerical simulation results 5MW WT: LSS torque response (left) and tower top/yaw bearing yaw moment response (right)